RXTE observations of the dipping low-mass X-ray binary 4U 1624-49

Lommen, D.; van Straaten, S.; van der Klis, M.; Anthonisse, B.

Link to publication

Astronomy
& Astrophysics

RXTE observations of the dipping low-mass X-ray binary 4U 1624–49

D. Lommen, S. van Straaten, M. van der Klis, and B. Anthonisse

Astronomical Institute "Anton Pannekoek", University of Amsterdam, and Center for High Energy Astrophysics,
Kruislaan 403, 1098 SJ Amsterdam, The Netherlands
e-mail: djplomme@science.uva.nl

Abstract. We analyse ~360 ks of archival data from the *Rossi X-Ray Timing Explorer* (*RXTE*) of the 21 h orbital period dipping low-mass X-ray binary 4U 1624–49. We find that outside the dips the tracks in the colour–colour and hardness-intensity diagrams (CDs and HIDs) are reminiscent of those of atoll sources in the middle and upper parts of the banana branch. The tracks show secular shifts up to ~10%. We study the power spectrum of 4U 1624–49 as a function of the position in the CD. This is the first time power spectra of this source are presented. No quasi-periodic oscillations (QPOs) are found. The power spectra are dominated by very low frequency noise (VLFN), characteristic for atoll sources in the banana state, and band limited noise (BLN) which is not reliably detected but may, uncharacteristically, strengthen and increase in frequency with spectral hardness. The VLFN fits to a power law, which becomes steeper when the source moves to the harder part of the CD. We conclude that 4U 1624–49 is an atoll source which in our observations is in the upper banana branch. Combining this with the high (0.5–0.7 L_{Edd}) luminosity, the long-term flux stability of the source as seen with the *RXTE All-Sky Monitor* (*ASM*), and with the fact that it is an X-ray dip source, we conclude that 4U 1624–49 is most likely a GX atoll source such as GX 3+1 and GX 9+9, but seen edge on.

Key words. accretion, accretion disks – stars: individual: 4U 1624–49 – stars: neutron – X-rays: stars

1. Introduction

The low-mass X-ray binary 4U 1624–49 was dubbed The Big Dipper because of the presence of periodic, 6 to 8 h duration intensity dips in the X-ray lightcurve (Watson et al. 1985). No periodic dips longer than ~1 h had been observed in other sources. This dipping is thought to be due to occultations of the central source by a thickened region of the accretion disc rim where the gas stream from the companion impacts upon the outer disc (see e.g. White & Swank 1982). Frank et al. (1987) suggested that the dips are due to cold clouds closer to the centre of the disc. However, their model predicts little dip activity for photon energies ≳6 keV, whereas the dips in 4U 1624–49 are detected up to 15 keV and even discernible above 15 keV (Smale et al. 2001). The orbital period of 4U 1624–49 is exceptionally long, 21 h or 5–25 times longer than that of other dipping sources. This corresponds to a much larger stellar separation and accretion disc radius, and it can be assumed to also account for the long duration of the dips.

4U 1624–49 also shows strong flaring activity on timescales of a few thousand seconds. While dipping is most clear in the energies below ~10 keV, flaring is not significant at energies below 8 keV (Smale et al. 2001). Balucińska-Church et al. (2001) presented a hardness-intensity diagram exhibiting a branch which they interpreted as similar to a Z-source flaring branch (see Hasinger & van der Klis 1989, for definitions).

In atoll sources in the banana state, the very low frequency noise (VLFN) can be fitted with a power-law shape, $P(\nu) \propto \nu^{-\alpha}$ (see Hasinger & van der Klis 1989), sometimes combined with a Lorentzian (e.g. Reerink et al. 2005; Di Salvo et al. 2003). The steepness of the power law increases as the source moves from the lower to the upper part of the banana. In this paper we study the colour–colour and hardness-intensity diagrams (CDs and HIDs) of 4U 1624–49 and look for features in the power spectra as a function of location in the CD. By investigating in particular the VLFN component, we find that 4U 1624–49 is consistent with being an atoll source which is in the banana state at the time of the observations.

2. Observations

In this work we analyse observations from the public *RXTE* archive. The data are from four proposals, spanning a period from January 1997 to November 1999. The log of these observations is presented in Table 1. We used data from the Proportional Counter Array (PCA; see Zhang et al. 1993, for instrument information, Jahoda et al. (1996) for in-orbit performance) on board *RXTE*, which consists of five co-aligned Proportional Counter Units (PCUs), sensitive in the energy

Table 1. *RXTE* observations of 4U 1624–49 used in this paper. The observations from P20068 and P20067 are from January 5 and 6 1997, respectively, and are taken together in our analysis. The observations from P20071 span 8 days in May 1997, and the observations from P30064 span 4 days in 1999. The count rate is taken in the energy range 2–60 keV. Typical background is 100 counts per second (c/s). The table also shows whether a certain observation contained *no* dip, *part* of a dip, or a *complete* dip. Observation 30064-01-03-00 is not used in our analysis, since it consists mainly of a dip.

Observation ID	Begin time (UTC)	Good time[a] (s)	Rate[b] (c/s)	Gain epoch	Dip?
20068-01-03-00	05/01/97 00:22	2820	926	3	no
20068-01-04-00	05/01/97 03:44	1620	997	3	no
20068-01-05-00	05/01/97 07:36	1080	1039	3	no
20068-01-06-00	05/01/97 10:52	914	994	3	no
20068-01-07-00	05/01/97 14:19	2700	971	3	no
20067-01-01-000	06/01/97 11:14	25 912	1021	3	no
20067-01-01-00	06/01/97 18:26	5468	1092	3	no
20067-01-01-01	06/01/97 20:44	24 250	960	3	no
20071-02-01-00	04/05/97 15:57	19 477	943	3	no
20071-02-01-02	06/05/97 10:46	5334	1001	3	no
20071-02-01-01	06/05/97 17:49	11 720	928	3	no
20071-02-01-03	11/05/97 18:47	16 828	890	3	no
30064-01-02-03	27/09/99 18:22	1269	865	4	no
30064-01-01-09	27/09/99 19:58	20 529	990	4	no
30064-01-01-04	28/09/99 03:09	14 792	1074	4	no
30064-01-01-08	28/09/99 09:13	15 376	912	4	part
30064-01-01-000	28/09/99 14:09	28 800	975	4	part
30064-01-01-00	28/09/99 22:09	2465	1108	4	no
30064-01-01-02	28/09/99 23:18	22 084	1067	4	no
30064-01-01-03	29/09/99 07:32	13 618	836	4	part
30064-01-01-010	29/09/99 12:30	28 800	987	4	no
30064-01-01-01	29/09/99 20:30	12 424	1025	4	no
30064-01-01-050	30/09/99 00:45	23 997	916	4	part
30064-01-01-05	30/09/99 07:25	15 547	974	4	no
30064-01-01-06	30/09/99 12:51	20 077	1059	4	no
30064-01-01-07	30/09/99 23:22	2300	857	4	no
30064-01-02-01	01/10/99 00:01	1200	881	4	no
30064-01-02-000	01/10/99 02:44	28 736	868	4	part
30064-01-02-00	01/10/99 10:43	8947	1067	4	no
30064-01-03-00	20/11/99 12:21	14 400	594	4	complete

[a] Total on-source observing time.
[b] Average, not corrected for the background, normalised to 5 PCUs.

range 2–60 keV, with a total effective area of approximately 6500 cm^2 and a field of view, delimited by collimators, of 1° FWHM. Each PCU contains three detector layers and in our analysis we used all the photons collected by the three layers taken together. We excluded data for which the source was less than 10 degrees above the horizon from the point of view of the satellite, and data for which the pointing offset was greater than 0.02 degrees. We also removed data drop outs and 1 s of data directly preceding and following them.

3. Analysis and results

3.1. Colour–colour and hardness-intensity diagrams

We produced background-subtracted lightcurves binned at 128 s using PCA Standard 2 mode data (16 s time resolution). The soft colour (SC) was defined as the ratio of the count rates in the bands 3.5–6.4 keV and 2.0–3.5 keV, the hard colour (HC) as the ratio of the count rates in the bands 9.7–16.0 keV and 6.4–9.7 keV. For the intensity, we took the total count rate in the 2.0–16.0 keV range. Hardness and intensity were normalised to the Crab values, as obtained during calibration observations close in time and in the same gain epoch (see for details e.g. van Straaten et al. 2003).

To allow for a better comparison of 4U 1624–49 with known atoll sources, data obtained during dips (see, e.g., Fig. 2 in Smale et al. 2001), where colours and intensity are affected by the obscuration process producing the dips, were excluded from the analysis. The resulting CD and HID are shown in Fig. 1.

We grouped the data into 3 large segments well separated in time. The observations of P20067 and P20068 spanned only 2 days and were taken together in our analysis. The result was then compared with the observations of P20071 (spanning 8 days) and P30064 (spanning 4 days; 30064-01-03-00 was not used, since it mainly consists of a dip) in the CDs and HIDs.

The shape of the CD suggests that the source is an atoll source in the banana state (Hasinger & van der Klis 1989). Most of the time, the source is in the lower banana (softer state); occasionally it moves through the banana to the harder upper banana region. By investigating the relation between the CD/HIDs and light curves, we found that the softer points in the lower banana are due to the persistent radiation that the source is normally emitting outside the dips, whereas the harder points come from occasional intensity flares.

Both the CD and HID show secular shifts (e.g. Di Salvo et al. 2003) consistent with the SC decreasing, and the HC and/or the intensity gradually increasing over the almost 3-yr period of the observations. The *RXTE All-Sky Monitor* (*ASM*, see Fig. 2) lightcurve shows no clear increasing trend, so we attribute the shift in the HID to a shift in SC. The colours change up to ~10%.

3.2. Power spectra

To study the power spectrum as a function of the position in the CD we created power spectra from all non-dip data obtained in the Good-Xenon mode. Previous experience with atoll sources shows (e.g. Di Salvo et al. 2003, 4U 1636–53) that the power spectra depend on the position of the source relative to the track but not on the track's location in the CD, i.e., its secular shifts. On this basis we shifted the colour–colour points of P20071 and P30064 to approximately coincide with those of P20067 and P20068. The data points of P20071 were shifted in SC by 4%, but not shifted in HC. The data points of P30064 were shifted in SC by 6.5%, and by −4% in HC. The result is shown in Fig. 3. We divided the CD into four regions, 1, 2, 3, and 4 (Fig. 3). These regions were chosen because the power

Fig. 2. *RXTE All-Sky Monitor* (*ASM*) lightcurve of 4U 1624–49, showing the day-by-day averages of the *ASM* counts.
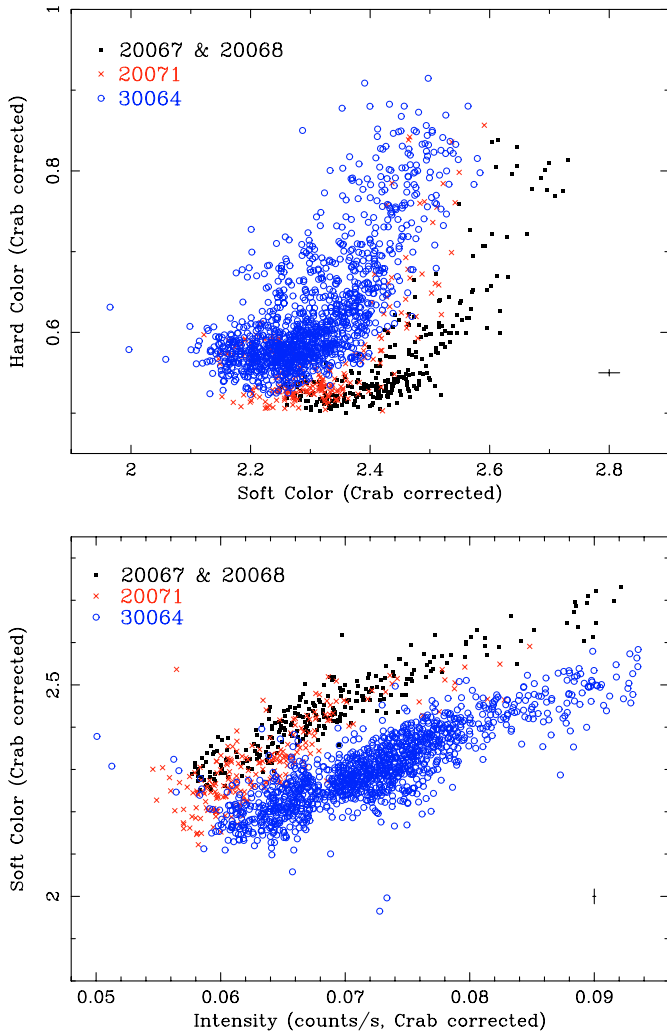

Fig. 1. Colour–colour diagram (upper panel) and hardness-intensity diagram (lower panel) of 4U 1624–49. The soft and hard colours are defined as the ratio of the count rate in the bands 3.5–6.4 keV/2.0–3.5 keV and 9.7–16.0 keV/6.4–9.7 keV, respectively. The intensity is defined as the source count rate in the energy range 2.0–16.0 keV. The soft and hard colours, as well as the intensity, are normalised to the Crab values. As indicated in each frame, different symbols indicate datasets from different observations, where P20067 and P20068 are taken together. Each data point corresponds to 128 s of data. Typical errors are shown.

Fig. 3. Same as the upper panel of Fig. 1, but here the data of P20071 and P30064 are shifted so that the tracks corresponding to the different proposals coincide. The selections 1, 2, 3, and 4 are used to create the power spectra.

spectra of atoll sources are observed to change when the source moves from the lower banana to the upper banana and back (see Hasinger & van der Klis 1989). For statistical reasons, the regions are quite large. A region corresponds to between 142 and 791 power spectra. After confirming that the power spectra in each region do not depend on the data segment, we calculated one average power spectrum for each region.

We used Good Xenon data, with data segments of 128 s and a time resolution of 1/8192 s ($\sim$125 μs), to produce Fourier power spectra, such that the lowest available frequency is 1/128 s and the Nyquist frequency is 4096 Hz. A Poisson noise level, estimated with the Zhang model (Zhang et al. 1995), was subtracted. For 4U 1630–47 it was found (Klein-Wolt 2004) that the Zhang model does produce the correct shape for the
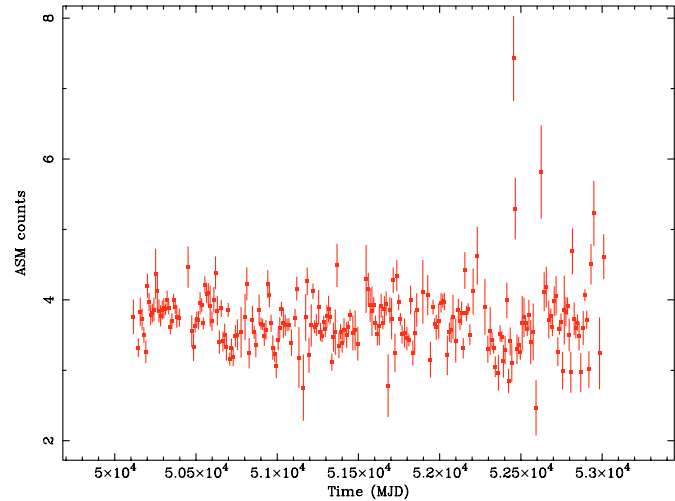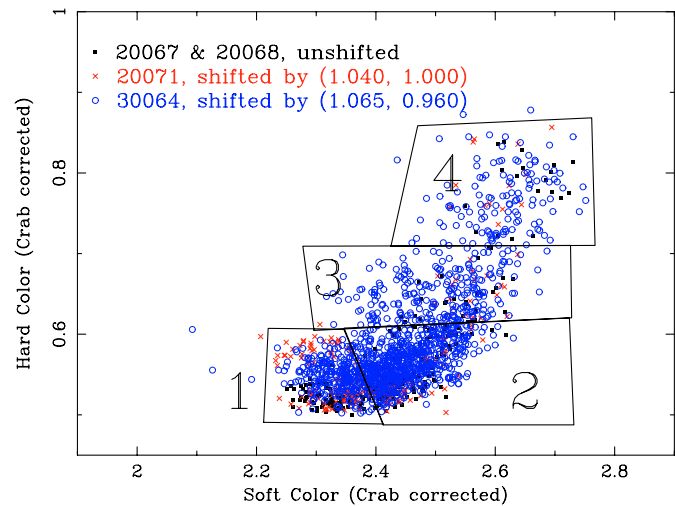
Poisson noise, but that the estimated level is slightly too high or too low. To correct for this, an aditional shift was introduced, where the scaling factor for the shift is determined in a (high) frequency range where no features are known to be present (see Klein-Wolt 2004, for the details of this method). In our analysis we determined the shift in the 3072–4096-Hz range and found it to be of order 10^{-7} in power in all cases, having a negligible effect on the results. We checked for features in the 3 to 4 kHz range by also creating power spectra with a Nyquist frequency of 8192 Hz and found none, justifying this range for the noise estimate.

We then made a fit to the average power spectrum for each region. We used a power law, in most fits combined with a Lorentzian, to fit the noise below 1 Hz, the "total VLFN." The power-law component is called VLFN as in Hasinger & van der Klis (1989), and the Lorentzian component is called "high VLFN" (see, e.g., Schnerr et al. 2003). In some cases another

significant (>3σ) Lorentzian was detected; this component is called the "band-limited noise (BLN)" (see, e.g., van Straaten et al. 2002). All high-VLFN and BLN features in the spectra are broad, and could be well described with zero-centered Lorentzians. Therefore we fixed the quality factor Q to 0. This results in the characteristic frequency ν_{max} of each Lorentzian component being equal to its half-width at half-maximum. The actual Lorentzian functions fitted were of the form

$$P(\nu; \nu_{max}, r) = \frac{r^2 \nu_{max}}{(\pi/2)\left[\nu_{max}^2 + \nu^2\right]}, \quad (1)$$

where r (the fractional root-mean-square (rms) integrated from 0 to ∞), and ν_{max} were the independent fit parameters.

We plot the power spectra and the fit functions in the power times frequency representation where power spectral density is multiplied with its Fourier frequency. The results are shown in Fig. 4 and in Table 2. All power spectra are dominated by the VLFN, which is fitted with a power law and a Lorentzian. The Lorentzian in region 3 is not significant. For this feature we calculated an upper limit to the rms. Also the total VLFN rms was calculated and is shown in Table 2. The feature in region 3 around 3000 Hz is not real; it is due to aliasing and disappears when a Nyquist frequency of 8 kHz instead of our usual 4 kHz is used. In region 4, we found a significant feature around 10 Hz which we attribute to the BLN. There seems to be a feature around 3 Hz as well, but this feature is not significant.

The steepness of the power law fitting the VLFN increases when the source moves from region 1 through to 4. This is what we expect from an atoll source in the banana state. Also the fractional rms is consistent with increasing as the hardness increases. The Lorentzian at 10 Hz in region 4 affects the index and rms of the power law only slightly. Fitting this region with a power law and only one Lorentzian gives $\alpha = 1.8 \pm 0.3$ and an rms of $1.8 \pm 0.3\%$, making this still the steepest and strongest power law of the four. We also made fits to the power spectra using a power law and no Lorentzians. This allows for a better comparison between region 3, which has no significant Lorentzians, and the other regions. The results of this are shown in Table 2. Also in this case steepness and rms increase as the source moves from 1 to 4. The fact that α does not increase when moving from region 1 to 2, may be a result of the choice of the regions, i.e., region 2 has the same hard colour as region 1. Finally we fitted the power spectra with the power-law steepness fixed to $\alpha = 1.7$, thus assuring that the power law fitting the VLFN does not fit to features at higher frequencies. We then find two Lorentzians in each region. The results are shown in Table 2. The rms of the power law still increases when the source moves to the harder part of the CD. Besides we note that the characteristic frequencies of the Lorentzians significantly increase when the source moves from region 1 to region 4, from 0.11 ± 0.02 to 0.20 ± 0.03 and from 1.6 ± 0.8 to 12^{+12}_{-5} for the high VLFN and the BLN, respectively.

4. Discussion

We analysed ~360 ks of archival *RXTE* data of 4U 1624–49 taken between January 1997 and November 1999.

The shape of the CD suggests that 4U 1624–49 is an atoll source, which is in the banana state at the time of the observations. We will investigate this suggestion in the light of the paper by Hasinger & van der Klis (1989) in which the two classes of LMXBs, atoll and Z sources, are first defined. They find that atoll sources differ from Z sources in:

- the absence of horizontal branch QPOs;
- the fact that the VLFN is less steep;
- the presence of clear wiggles in the VLFN;
- the fact that they often show very strong high-frequency noise (BLN in this paper, after e.g. van Straaten et al. 2002), which is arguably different from normal-branch/flaring-branch QPOs in Z sources.

We first note that no QPO is detected in the power spectra of 4U 1624–49 (see also Smale et al. 2001), and that the power spectra also show wiggles (the high-VLFN components) in the VLFN. Balucińska-Church et al. (2001) argued that during flare evolution systematic changes clearly take place in the HIDs very similar to the flaring branch of Z-track sources displayed on similar diagrams. Hasinger & van der Klis find a VLFN power-law index in the range $1.3 < \alpha < 1.9$ on the flaring branch, and $0.9 < \alpha < 1.5$ on the banana branch. When we leave the power-law index free in our fits, we find it to be in the range $1.0 < \alpha < 1.4$ (except in the case where also a significant BLN feature is found, see Sect. 3.2). From these arguments we conclude that 4U 1624–49 should be classified as an atoll source in the banana branch. Consistent with this, the values of α and the fractional rms of the VLFN tend to increase when moving to the upper right in the CD, like other atoll sources moving up the banana branch.

The banana branch is usually subdivided into the lower left banana (LLB), the lower banana (LB), and the upper banana (UB, see again Hasinger & van der Klis 1989, for definitions). Reerink et al. (2005) in their study of GX 3+1, GX 9+1, and GX 9+1 propose to define as a boundary between the LB and the UB the point where the trends of the power spectral components as a function of position in the branch change. The most notable trend changes in their study are those in the high-VLFN rms, which changes from a flat or slightly decreasing trend to an increasing trend, and that in the BLN rms, which changes from a decreasing trend to a flat or slightly increasing trend. Comparing our results to theirs (see Fig. 5), we find that 4U 1624–49 is in the UB.

In regions 1, 2, and 4, we found a significant (larger than 3σ) Lorentzian with a characteristic frequency in the range of ~0.11 to ~0.16 Hz, a high-VLFN component. The fractional rms of this Lorentzian ranged from ~1.6% to 2.8%. For region 3, we could set an upper limit to a similar Lorentzian with a fractional rms of 1.9% (95% confidence). These bumps in the VLFN are probably the same as those reported for the bright atoll sources GX 13+1 (Schnerr et al. 2003, ~3% rms at 1 Hz), and e.g. GX 9+9 and GX 9+1 (Reerink et al. 2005, ~2% up to ~4% at ~0.1 Hz). We also found a significant Lorentzian at 10 Hz in region 4. This is curious, since for other atoll sources, the BLN component at higher frequencies becomes weaker when the source moves to the upper banana. On the other hand, some atoll sources in the banana state show a QPO around 6 Hz
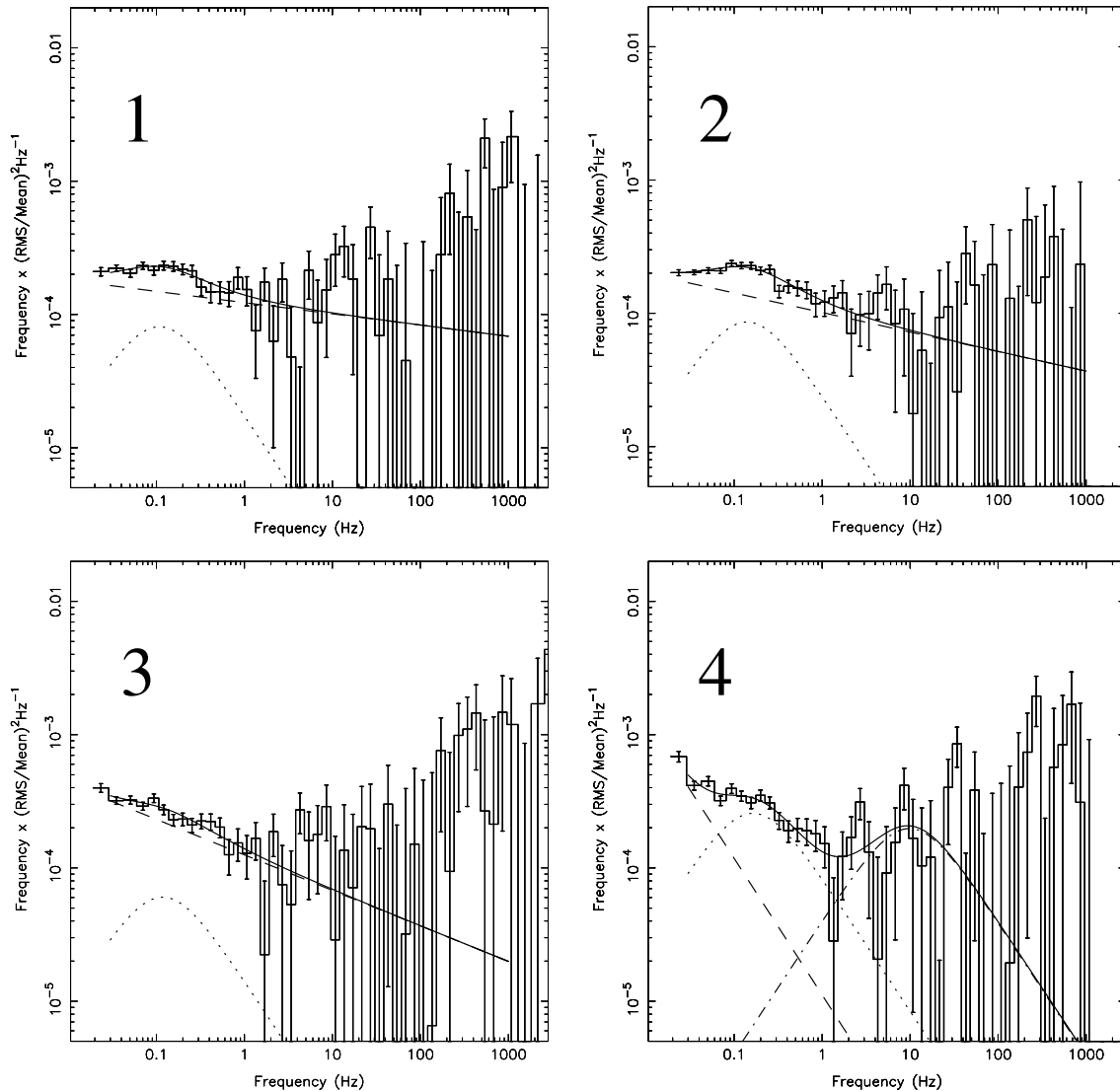
Fig. 4. Power spectra and fit functions in the power-spectral density times frequency representation (see Sect. 3.2) of regions 1 to 4 (Fig. 3) for fits with a power law plus Lorentzians with only Q of the Lorentzians fixed (at 0). The different components of the fits, where applicable, are as follows: *dashed line*: power law; *dotted line*: first Lorentzian; *dot-dashed line*: second Lorentzian. The sum of these components, i.e., the full fit, is plotted with a solid line. For the details of the different components, see Table 2.

when the source is at the tip of the upper banana. We searched for this QPO by applying the analysis outlined in Sect. 3.2 to the top-most part of region 4, but did not find it.

When using a power law with index α fixed to 1.7 to fit the "low" VLFN, all four regions show a significant BLN component. However, whereas for other sources the characteristic frequency of the BLN tends to decrease as the source moves to the upper banana, in 4U 1624–49 this frequency increases. Also, the BLN frequency never reaches values of several 10 Hz, such as in most of the atoll sources (including GX 13+1, Schnerr et al. 2003, up to 30 Hz; and GX 9+9 and GX 3+1, Reerink et al. 2005, up to 60 Hz and 24 Hz, respectively).

We observed secular shifts in the colour–colour and hardness-intensity diagrams. Shifts like these are also observed in some Z sources (Smale et al. 2003; Kuulkers et al. 1994; Kuulkers et al. 1996, and references therein), and in the atoll sources 4U 1636–53 (Prins & van der Klis 1997;

Di Salvo et al. 2003) and GX 13+1 (Schnerr et al. 2003). The shifts in 4U 1624–49 are most clear in the colours, up to ∼10%, with little difference between HC and SC. The intensity of 4U 1624–49 is rather stable, as seen with the *ASM* (Fig. 2). In 4U 1636–53, the shifts in colours are only a few per cent, whereas the shift in intensity is up to ∼20%. The shifts in GX 13+1 are up to ∼40% in HC, ∼7% in SC, whereas there is only a shift in intensity in the upper-most part of the banana (up to ∼20%). The shifts in 4U 1624–49 towards higher HC and/or lower SC seem to be rather gradual over the almost 3-yr period of the observations, whereas GX 13+1 moves back and forth between higher and lower HC on a time scale of weeks. The shift in 4U 1636–53 is not gradual at all, this source appears to "jump" from one state to another as is reflected in the lower kHz QPO frequency vs. count rate diagram (Fig. 2 in Di Salvo et al. 2003). This may indicate a different source for the secular shifts in 4U 1636–53 as opposed to GX 13+1 and

Table 2. Parameters of the fit components. In all cases, the quality factor Q of the Lorentzians was fixed to 0. All the values shown are of components detected at better than 3σ (based on the error in the power integrated from 0 to ∞), unless otherwise stated.

Region	1	2	3	4
Rate^a (10^2 c/s)	7.1 ± 0.3	7.1 ± 0.3	6.9 ± 0.3	8.2 ± 0.3
# power spectra	416	791	262	142
Background^b (10^2 c/s)	1.17 ± 0.11	1.03 ± 0.10	0.93 ± 0.09	1.00 ± 0.10
all parameters left free				
VLFN α	1.09 ± 0.03	1.14 ± 0.03	1.27 ± 0.03	2.0 ± 0.2
VLFN rms^c (%)	2.62 ± 0.10	2.59 ± 0.07	3.35 ± 0.05	3.44 ± 0.15
high VLFN ν_{max}	0.11 ± 0.02	0.14 ± 0.02	0.12	0.16 ± 0.03
high VLFN rms (%)	1.58 ± 0.16	1.61 ± 0.12	$<1.9^d$	2.84 ± 0.22
total VLFN rms (%)	3.06 ± 0.06	3.05 ± 0.05	$3.3 < \text{rms} < 5.3$	4.47 ± 0.06
BLN ν_{max}	–	–	–	10 ± 6
BLN rms (%)	–	–	–	2.5 ± 0.4
χ^2/d.o.f.	120/95	79/95	102/97	104/93
power law only				
α	1.065 ± 0.016	1.084 ± 0.012	1.22 ± 0.02	1.32 ± 0.03
rms^c (%)	3.02 ± 0.03	3.00 ± 0.02	3.61 ± 0.04	4.18 ± 0.06
χ^2/d.o.f.	145/95	129/95	100/95	127/95
fixed power law				
VLFN α	1.7 (fixed)	1.7 (fixed)	1.7 (fixed)	1.7 (fixed)
VLFN rms^c (%)	1.68 ± 0.09	1.82 ± 0.06	2.76 ± 0.10	3.65 ± 0.11
high VLFN ν_{max} (Hz)	0.107 ± 0.015	0.131 ± 0.011	0.14 ± 0.02	0.20 ± 0.03
high VLFN rms (%)	2.39 ± 0.08	2.38 ± 0.06	2.39 ± 0.09	2.37 ± 0.12
total VLFN rms (%)	2.93 ± 0.04	2.99 ± 0.03	3.65 ± 0.04	4.35 ± 0.04
BLN ν_{max} (Hz)	1.6 ± 0.8	2.6 ± 1.0	6 ± 3	12^{+12}_{-5}
BLN rms (%)	1.89 ± 0.16	1.79 ± 0.15	2.3 ± 0.3	2.5 ± 0.5
χ^2/d.o.f.	130/94	81/94	104/94	107/94

Errors correspond to $\Delta\chi^2 = 1$.

^{a} PCA count rate, 5 PCUs, not corrected for the background. Counting statistics errors are quoted.

^{b} Averaged background. Counting statistics errors are quoted.

^{c} rms amplitude calculated in the frequency range 0.01–1.0 Hz.

^{d} 95% confidence upper limit.

4U 1624–49. Schnerr et al. (2003) propose secular geometry changes such as precession as possible sources for the secular shifts, which would account for the gradual change. They assume a head-on view to GX 13+1 (and a jet scenario) to explain the large shift in HC. 4U 1624–49 is a dipping source and thus has a high inclination ($60° \lesssim i \lesssim 75°$ according to Frank et al. 1987), which might explain the much smaller shift in HC for this source. For more insight in the processes behind the secular shifts, more data on different sources and per source is necessary, and thus long-term X-ray observations of several sources are recommended.

5. Conclusion

Outside the dips, 4U 1624–49 shows properties that are mostly consistent with those of an atoll source at high luminosity: a "middle" and upper banana branch in CD/HIDs, secular shifts of the tracks, a power spectrum dominated by a few % rms VLFN that becomes stronger and steeper at harder colours. All this is very similar to what is observed in "GX atoll sources"

such as GX 3+1 and GX 9+9 (Reerink et al. 2005). However, to the extent that it can be detected the characteristic frequency of the BLN may increase, rather than decrease as in those sources. During our observations, the luminosity of 4U 1624–49 was $(1.5-1.7)\times10^{38}$ erg s^{-1} (Smale et al. 2001; Balucińska-Church et al. 2001), i.e., $\sim0.5-0.8L_{Edd}$, which is in accordance with luminosities inferred for the GX atoll sources. Combining all this with the fact that 4U 1624–49 shows periodic dips and is rather stable in flux we conclude that 4U 1624–49 most likely is a GX atoll source seen edge on. The fact that the BLN in this source has a characteristic frequency that is atypically low and monotonically increasing may be related to this unusual inclination of the source, perhaps because the innermost region of the disk where the highest frequencies originate is obscured by structure slightly further out, e.g. a puffed-up disk region associated with the radiation-pressure dominated region.
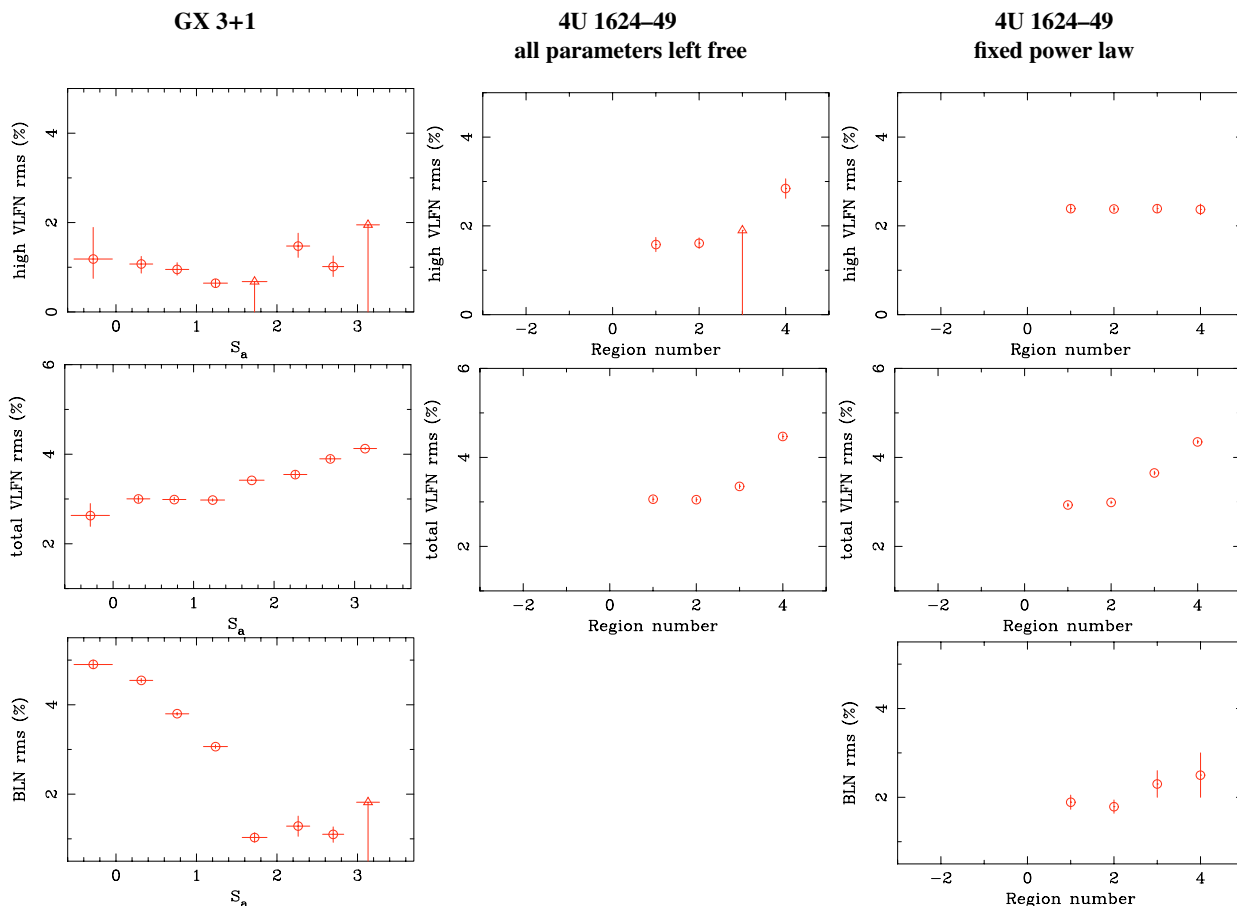
Fig. 5. Comparison between the trends in the high VLFN rms, the total VLFN rms, and the BLN rms of GX 3+1 and 4U 1624–49. The values of GX 3+1 are taken from Reerink et al. (2005) and are representative for the bright GX sources GX 9+9, GX 9+1, and GX 3+1. Note that Reerink et al. (2005) use so-called S_a values to define their intervals, where $S_a > 1.5$ corresponds to GX 3+1 being in the UB. We plotted our results on a similar scaling for easier comparison. Because no significant BLN component is found for 4U 1624–49 in three of the four regions when all parameters are left free in the fit, we also show the values for the fits in which the power-law index was fixed. We find that based on these criteria 4U 1624–49 is in the UB throughout the observations.

References

Balucińska-Church, M., Barnard, R., Church, M. J., & Smale, A. P. 2001, A&A, 378, 847

Di Salvo, T., Méndez, M., & van der Klis, M. 2003, A&A, 406, 177

Frank, J., King, A. R., & Lasota, J.-P. 1987, A&A, 178, 137

Hasinger, G., & van der Klis, M. 1989, A&A, 225, 79

Jahoda, K., Swank, J. H., Giles, A. B., et al. 1996, in EUV, X-Ray, and Gamma-Ray Instrumentation for Astronomy VII, ed. O. H. Siegmund, & M. A. Gummin, Proc. SPIE, 2808, 59

Klein-Wolt, M. 2004, Ph.D. Thesis, University of Amsterdam

Kuulkers, E., van der Klis, M., Oosterbroek, T., et al. 1994, A&A, 289, 795

Kuulkers, E., van der Klis, M., & Vaughan, B. 1996, A&A, 311, 197

Prins, S., & van der Klis, M. 1997, A&A, 319, 498

Reerink, T. J., Schnerr, R. S., van der Klis, M., & van Straaten, S. 2005, A&A, submitted

Schnerr, R. S., Reerink, T., van der Klis, M., et al. 2003, A&A, 406, 221

Smale, A. P., Church, M. J., & Bałucińska-Church, M. 2001, ApJ, 550, 962

Smale, A. P., Homan, J., & Kuulkers, E. 2003, ApJ, 590, 1035

van Straaten, S., van der Klis, M., di Salvo, T., & Belloni, T. 2002, ApJ, 568, 912

van Straaten, S., van der Klis, M., & Méndez, M. 2003, ApJ, 596, 1155

Watson, M. G., Willingale, R., King, A. R., Grindlay, J. E., & Halpern, J. 1985, in International Astronomical Union Circular, 2

White, N. E., & Swank, J. H. 1982, ApJ, 253, L61

Zhang, W., Giles, A. B., Jahoda, K., et al. 1993, in EUV, X-Ray, and Gamma-Ray Instrumentation for Astronomy IV, ed. O. H. Siegmund, Proc. SPIE, 2006, 324

Zhang, W., Jahoda, K., Swank, J. H., Morgan, E. H., & Giles, A. B. 1995, ApJ, 449, 930